Journal of Materials Chemistry A

Accepted Manuscript

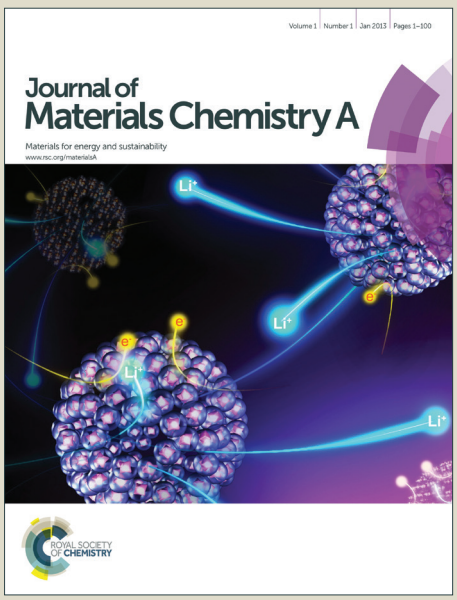

ROYAL SOCIETY OF CHEMISTRY

www.rsc.org/materialsA

Journal of Materials Chemistry A

ARTICLE

Fabrication of superhydrophobic Au-Zn alloys surface on zinc substrate for roll-down, self-cleaning and anti-corrosion properties

Received 00th January 2015,
Accepted 00th January 2015

DOI: 10.1039/x0xx00000x

www.rsc.org/

Yuanyuan Cheng[a], Shixiang Lu[*a], Wenguo Xu[*a], Huidong Wen[b] and Juan Wang[a]

Superhydrophobic Au-Zn alloys surfaces have been fabricated successfully on zinc substrate via chemical substitution deposition and subsequent annealing treatment. The resulting surfaces exhibited remarkable superhydrophobicity with a WCA of 170 ±2º and a WSA smaller than 1º without any organic modification. The surface morphologies and chemical compositions were investigated using field emission scanning electron microscopy (FESEM) equipped with an energy-dispersive spectroscopy (EDS), x-ray powder diffraction (XRD) and x-ray photoelectron spectroscopy (XPS), and the surface roughness was analyzed by atomic force microscopy (AFM). The theoretical mechanism for superhydrophobicity and wettability were also analyzed respectively. The surface wettability changed from superhydrophilicity to superhydrophobicity with stable Cassie-Baxter state via thermal treatment, which caused the generation of Au-Zn alloys (including $AuZn_3$ and AuZn) and ZnO, and the formation of micro-/nano- binary architectures. The resulting superhydrophobic Au-Zn alloys surfaces exhibited exquisite roll-down, self-cleaning, and excellent anti-corrosion properties, and also had firm mechanical property about 10 N, and this might have important values for more potential applications. The corrosion current density was reduced by more than 2 order of magnitude for the resulting superhydrophobic surface in comparison with the untreated zinc surface and this should owe to the contribution of Au-Zn alloys on the surface.

Introduction

Wettability and adhesiveness phenomena, owing to the interactions between liquids and solid surfaces on hydrophobic and hydrophilic surfaces, have been extensively studied over the last decades and have been verified its various potential applications in our daily life.[1-3] Especially, superhydrophobic surfaces have attracted tremendous attention due to their variety of special applications in the fields of self-cleaning, anti-icing, anti-corrosion, anti-biofouling, water-oil separation and drug delivery, etc.[4-9] These surfaces with a static water contact angle (WCA) greater than 150º and a sliding angle (SA) lower than 10º, have considerable potential values in fundamental research and industrial applications. The phenomenon of superhydrophobicity has been explained by two renowned theories proposed by Wenzel[10] and Cassie[11] independently. Wenzel theory recognizes that surface roughness increases the available surface area of the solid, and the droplet follows the roughness surface and fills the asperities. Therefore, the water droplet sticks to the surface completely, and thus the Wenzel state displays a very high adhesive property. The Cassie theory, on the other hand, postulates that the superhydrophobic nature of a rough surface is caused by microscopic pockets of air remaining trapped below the liquid droplet, leading to a composite interface. So in this case, water droplet does not penetrate into the rough surface, and it just rests on top of the asperities. Obviously, the Cassie state provides large WCA and at the same time has low contact angle hysteresis, leading to a roll-down superhydrophobic surface.[12-14] It is noteworthy to mention that rolling-down behaviour of superhydrophobic surface has useful application in self-cleaning.

Inspired by the potential application of superhydrophobic surfaces, many researchers have fabricated these surfaces successfully by electrodeposition,[15] anodization,[16] laser treatment,[17] chemical vapour deposition,[18] layer-by-layer deposition,[19] chemical deposition,[20] sol-gel method,[21] template[22] and one-step immersion process[23,24] etc. However, most of them require organic reagent as the modifier; yet, the organic modification will restrict the intrinsic property of the metal substrates, such as excellent electro-conductivity, thermal conductivity and high temperature resistance. In addition, these methods have certain limitations, such as tedious fabrication, severe condition and expensive equipments, etc. Our group had fabricated superhydrophobic Au-$AlAu_4$-Al_2O_3 surfaces on aluminium substrate via electroless galvanic deposition of $HAuCl_4$ aqueous solution and annealing treatment without any organic modification.[6] Therefore, we hope to fabricate other

[a] School of Chemistry, Beijing Institute of Technology, Beijing 100081, P.R. China.
E-mail: shixianglu@bit.edu.cn; xuwg60@bit.edu.cn;
Fax: +86 10 68912631; Tel: +86 10 68912667
[b] MXTronics Corporation, Beijing Microelectronic Technology Institute, Beijing 100076, P.R. China.
† Electronic Supplementary Information (ESI) available. See
DOI: 10.1039/x0xx00000x

alloy surfaces with superhydrophobicity on zinc substance without low surface energy materials to modify.

Zinc, as an important engineering material, has received much attention in industries due to its high diathermanous and electric performance. In the past few years, researchers have discovered many methods to fabricate superhydrophobic surfaces on zinc substrate. For example, Li *et al.*[25] reported that superhydrophobic surfaces with controlled sliding angles on zinc substrates had been fabricated via a simple hydrothermal process and the subsequent modification of stearic acid, and the hydrothermal process could be regulated by changing the concentration ratio of H_2O_2/NaOH and temperature to tune the surface morphologies. Sun *et al.*[26] fabricated a superhydrophobic surface with a water contact angle of 165.3º and a tilting angle of 2º on zinc substrate by electrochemical processing using a mixed electrolyte composed of NaCl and $NaNO_3$, followed by overcoating with a fluorinated polymer, and the fabrication process was based on the electrochemical processing of Zn under an applied electric field. Yu *et al.*[27] presented a simple approach for preparation of superhydrophobic and oleophobic surface on zinc substrate by chemical etching, hydrothermal reaction and subsequent chemical modification with perfluorooctanoic acid anhydrous ethanol solution. Wang *et al.*[28] innovatively proposed a facile and controllable way to prepare a superhydrophobic Zn/ZnO film on zinc substrate and the lotus-like hierarchical Zn/ZnO micro/nano structure could be acquired and tailored under a wide range of reaction conditions by controlling the reaction temperature and duration; the as-prepared superhydrophobic samples showed good thermal stability (under 200℃) and recoverability. Zhang *et al.*[29] prepared a superhydrophobic ZnS film by a simple solvothermal method using Zn foil and S powder as raw materials in an absolute ethanol solution at 160℃ for 8 h and the ZnS film exhibited excellent superhydrophobicity owing to its special nano-flake structure. But these methods had some drawbacks. For instance, most of them employed organic modification, which would restrict the intrinsic property of the zinc metal substrates. Additionally, these methods were not convenient because the manipulation necessitated costly instrument and power supply. Hence, these drawbacks inspired us to develop a facile, convenient, direct, simple, nontoxic, and without organic modification method to prepare superhydrophobic surface on zinc substrates for more potential applications.

Here, we developed the firm superhydrophobic Au-Zn alloys (including $AuZn_3$ and AuZn) surfaces for exquisite roll-down, self-cleaning, excellent anti-corrosion properties by simple chemical substitution reaction using zinc substrate and chloroauric acid aqueous solution as the starting materials under mild conditions, and then followed by annealing treatment. Appreciably, the procedure did not require any additional layer of low surface energy material. The surfaces were formed through etching with 1 mol/L NaOH alkaline solution for 5 min and then immersion in 5 mmol/L $HAuCl_4$ aqueous solution for 20 min and finally annealing in an oven at 160℃ for 30 min. Both of the generation of Au-Zn alloys (including $AuZn_3$ and AuZn) and ZnO, and the surface micro-/nano- binary architectures were important for superhydrophobicity.

Experimental

Materials

Chloroauric acid tetrahydrate ($HAuCl_4 \cdot 4H_2O$, Au ≥ 47.8 %), sodium hydroxide (NaOH, 96.0 %), ethanol (CH_3CH_2OH, 99.7 %) and sodium chloride (NaCl, 99.5 %) were analytic grade reagents without further purification and were purchased from Sinopharm Chemical Reagent Co., Ltd. Zinc sheets (99.9 %) were obtained from Beijing Nonferrous Metal Research Institute. Soils were from Beijing Institute of Technology.

Sample preparation

Zinc sheets with size of 1.0 cm × 1.0 cm × 0.1 cm were successively washed in an ultrasonic bath with ethanol and deionized water for 10 min respectively to remove surface grease. Subsequently, they were etched with 1 mol/L NaOH alkaline solution for 5 min and followed by rinsing with deionized water. Then, the samples were set vertically in an unplasticized poly vinyl chloride (UPVC) tube without a bottom as shown in our previous report,[6,17] and then were immersed in 5 mmol/L $HAuCl_4$ aqueous solution for 20 min at room temperature and dried in air. Finally, the samples were annealed in an oven at 160℃ for 30 min. All the treated samples were rinsed thoroughly with deionized water and dried in air for several minutes prior to the next step.

The influences of different preparation conditions, including etching time, immersion time, annealing time and annealing temperature, on wettability were investigated respectively, and the detailed results can be found in the supplementary information as shown in Fig. S1, Fig. S2, Fig. S3 and Fig. S4. The optimum conditions were conducted for preparing superhydrophobic surfaces.

Here, six different samples were prepared for our further study. Table 1 lists the WCA, WSA and characteristics of sample surfaces with different preparation process. Etch, Immersion and Anneal denote the samples after etching with 1 mol/L NaOH solution for 5 min, immersion in 5 mmol/L $HAuCl_4$ solution for 20 min and annealing in an oven at 160℃ for 30 min, respectively. Y and N signify performing the corresponding process and without performing, respectively.

Samples	Etch	Immersion	Anneal	WCA	WSA	Characteristics
1	N	N	N	54 ±2º	-	Hydrophobicity
2	Y	N	N	16 ±2º	-	Hydrophobicity
3	Y	Y	N	4 ±2º	-	Superhydrophilicity
4	Y	Y	Y	170 ±2º	< 1º	Superhydrophobicity
5	Y	N	Y	109 ±2º	-	Hydrophobicity
6	N	Y	Y	122 ±2º	-	Hydrophobicity

Table 1. The WCA, WSA and characteristics of sample surfaces with different preparation process. Etch, Immersion and Anneal denote the samples after etching with 1 mol/L NaOH solution for 5 min, immersion in 5 mmol/L $HAuCl_4$ solution for 20 min and annealing in an oven at 160℃ for 30 min, respectively. Y and N signify performing the corresponding process and without performing, respectively. The '-' means no WSA and adhering to the surface always.

Sample characterization

The surface morphologies were characterized using a field emission scanning electron microscope (FESEM, S-4800, HITACHI, Japan) equipped with an energy-dispersive spectroscopy (EDS, INCA Energy, Oxford CO, Japan). The nano-textured surfaces were characterized by atomic force microscope (AFM, D3100, Veeco, USA) with a conventional rectangular cantilever in tapping mode with the scanning rate of 0.1 Hz. The crystal structure was determined by x-ray powder diffractometer (XRD, D8 Advance, Bruker, Germany) with Cu *Kα* radiation at a continuous scanning mode (40 kV, 40 mA, and λ = 0.15418 nm) and scanning rate of 3 º/min. X-ray photoelectron spectrometer (XPS, PHI Quantera-II, Ulvac-Phi, Japan) was employed to characterize the surface compositions of the resulting surfaces using 25 W Al *Kα* (1486.6

eV) x-ray as the excitation source. The static water contact angles (WCAs) and sliding angles (SAs) were measured by remote computer-controlled goniometer system (FTÅ 200, Dataphysics Inc., USA) equipped with a video camera (Canon) and a tilting stage. SAs were measured by slowly tilting the sample stage until the water droplet started moving. Water droplets (8 μL) were carefully dropped onto the surfaces, and the average value of five measurements obtained at different positions was used as the final CA. All values of each sample were in a range of ±2º. The electrochemical measurements were conducted in 3.5 wt% NaCl aqueous solutions at room temperature using electrochemical workstation (CHI 760E, CH Instruments Inc., China). The electrochemical corrosion tests were carried out using a three-electrode configuration with platinum as the counter electrode, saturated calomel as the reference electrode, and the samples with an exposed area of 1 cm^2 as the working electrode. The polarization curves were obtained at a sweep rate of 2 mV/s. Tribological property was evaluated using a UMT Universal Mechanical Tester (UMT-2, Bruker, USA). The tribology experiment was conducted by a load, which ranged from 5 N to 20 N using a sharp diamond drill. The moving rate of the diamond drill during the scratch process was 0.017 mm/s and the one-way scratch length was 5 mm. The relevant experimental parameters were obtained using a realtime control computer and data analysis software.

Results and discussion

Wettability

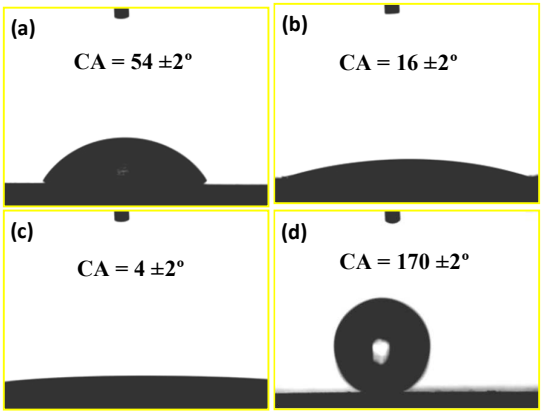

Fig. 1. Optical images of WCAs on different surfaces: untreated zinc surface (a), sample surface after etching with 1 mol/L NaOH solution for 5 min (b), superhydrophilic surface after immersion in 5 mmol/L $HAuCl_4$ solution for 20 min (c), and superhydrophobic surface after annealing in an oven at 160℃ for 30 min (d).

Fig. 1 shows the images of static water contact angles on the surfaces of sample 1, 2, 3 and 4 respectively, which clearly demonstrates the changes of wettability on the different sample surfaces. The WCA of the untreated zinc surfaces is approximately 54 ±2º, indicating hydrophilicity. After etching with 1 mol/L NaOH solution for 5 min, the WCA decreases to 16 ±2º, indicating more hydrophilicity. After immersion in 5 mmol/L $HAuCl_4$ solution for 20 min, the surface exhibits superhydrophilicity prior to annealing treatment. The water droplets completely spread on the surfaces with a WCA of approximately 4 ±2º. Finally, after annealing treatment in an oven at 160℃ for 30 min, the characteristic of the surface successfully changes from superhydrophilicity to superhydrophobicity, with a WCA of 170 ±2º and a WSA smaller than 1º. The water droplet can stand on the surface without any sticky behaviour, indicating the low contact angle hysteresis and low adhesive property, which will benefit the roll-down and self-cleaning properties. These results clearly demonstrate that etch, immersion and anneal processes are all important for the fabrication of superhydrophobic surfaces.

Surface morphology

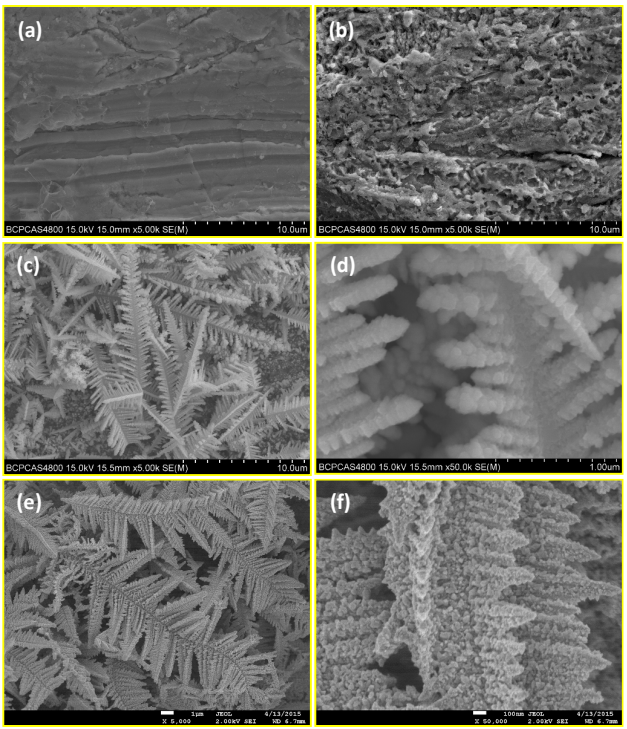

Fig. 2. SEM images: untreated zinc surface (a), sample surface after etching with 1 mol/L NaOH solution for 5 min (b), superhydrophilic surface after immersion in 5 mmol/L $HAuCl_4$ solution for 20 min (c and d), and superhydrophobic surface after annealing in an oven at 160℃ for 30 min (e and f). The magnification of (a), (b), (c), (e) is × 5 K and that of (d), (e) is × 50 K.

Fig. 2 presents SEM images on the surfaces of sample 1, 2, 3 and 4 respectively, clearly revealing the different surface morphologies and nano-sized particle clusters arrangement on the surfaces. In Fig. 2(a), untreated zinc sample displayed relatively smooth surface on which there were only some inherent scratches. However, sample 2 appeared to present a rough surface with amount of irregular, fragmentized and cracked surface textures as shown in Fig. 2(b), and these crumbling textures could be attributed to the result of the destruction by etching with 1 mol/L NaOH aqueous solution for 5 min. Fig. 2(c) revealed the rougher surface morphology of the sample after immersion in 5 mmol/L $HAuCl_4$ aqueous solution for 20 min. The surface was covered by many dendritic structures at random, which could be ascribed to elemental Au from electroless galvanic deposition and that can be distinctly observed in the XRD pattern (Fig. 5c). From the magnification of an individual dendrite as shown in Fig. 2(d), we can clearly see that Au dendrite was composed of a pronounced trunk and numerous leaves with size of about 0.5 μm to 1 μm. After annealing treatment as shown in Fig. 2(e), the dendritic structures were still presented and became stronger and tighter.

In addition, a large amount of nano-sized particle clusters emerged on the leaves as shown in Fig. 2(f), and this may be due to the generation of Au-Zn alloys via the thermal treatment, which can be observed from the XRD and XPS spectra in Fig. 5(d) and Fig. (6). Obviously, the micro-/nano- binary architectures were formed successfully on zinc substrate, which were similar to the micro- and nano- hierarchical structures on lotus leaf with superhydrophobicity.[30-34] Such micro-/nano-binary architectures were favourable for trapping air within the structures when water droplets were placed on the surface. So the dispensing of water droplet on the surface belonged to the Cassie-Baxter state, and droplet couldn't penetrate into the surface due to the presence of air pockets. Accordingly, the water droplet on the superhydrophobic surface rendered high WCA and became non-sticky. Thus, water droplet could roll down from the surface.

Surface roughness

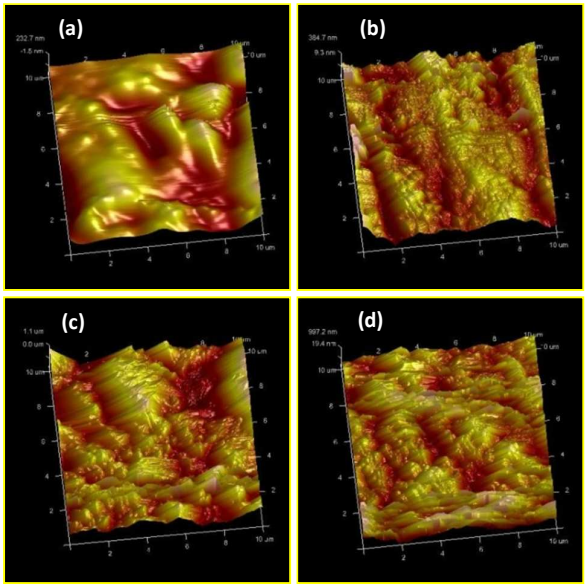

Fig. 3. 3-D AFM topology images: (a) sample 1, (b) sample 2, (c) sample 3 and (d) sample 4.

Samples	R_q (nm)	R_a (nm)	R_{max} (nm)
1	65.8	51.9	512
2	101	78.4	1220
3	289	226	2080
4	269	211	2690

Table 2. Roughness parameters: R_q (root-mean-square roughness), R_a (average roughness), and R_{max} (maximum peak-to-valley height) of surfaces of sample 1, sample 2, sample 3 and sample 4 respectively.

Surface roughness is important for wettability. So, atomic force microscopy (AFM) was employed to scan the surface topologies and analyze the surface roughness over an area of $10 \times 10\ \mu m^2$. Table 2 lists the values of R_q (root-mean-square roughness), R_a (average roughness), and R_{max} (maximum peak-to-valley height) of sample 1, 2, 3, and 4 respectively. Fig. 3 presents the three-dimensional (3-D) AFM surface topologies of the untreated zinc surface (sample 1), surface after etching process (sample 2), surface after immersion process (sample 3) and surface after annealing treatment (sample 4) respectively. According to Fig. 3(a) and Table 1, the untreated zinc surface was relatively smooth, with values of R_q and R_a both below 70 nm. For sample 2, the surface topology became rougher and the surface morphologies turned into numerous hills. After immersion process, the surface roughness increased dramatically and the surface morphologies became mountains-and-valleys topologies. For sample 4, the surface morphologies still presented mountains-and-valleys topologies, which were analogous to that of sample 3. The data of Table 2 reveals that sample 3 and sample 4 have similar R_q (289 vs 269 nm) and R_a (226 vs 211 nm). These roughness parameters of the superhydrophobic surface were in accord with Boscher's results[35] and similar to the roughness values reported by Lo *et al*.[36]

However, although the surface roughnesses of sample 3 and sample 4 were similar, their WCAs and WSAs were very different obviously. From the data of Table 1 and Fig. 1(c) and (d), we can clearly see that the surface characteristics of sample 4 completely transformed from superhydrophilicity to superhydrophobicity with WCA of 170 ±2º and WSA smaller than 1º. Considering the superhydrophobicity and low contact angle hysteresis exhibited in sample 4, we believed that the surface roughness was enough to render high air-trapping capacity within water/surface interface. The appearance of nano-sized particle clusters was very important for the formation of micro-/nano- binary architectures, leading to different water/surface contact behaviours of sample 3 and 4. It is well known that the wettability of solid surfaces can be controlled by surface topography and/or surface chemistry. The excellent superhydrophobicity of sample 4 was presumably due to both of the contributions. Then we further discuss the influence of surface composition, deciding the surface chemical environment.

Surface composition

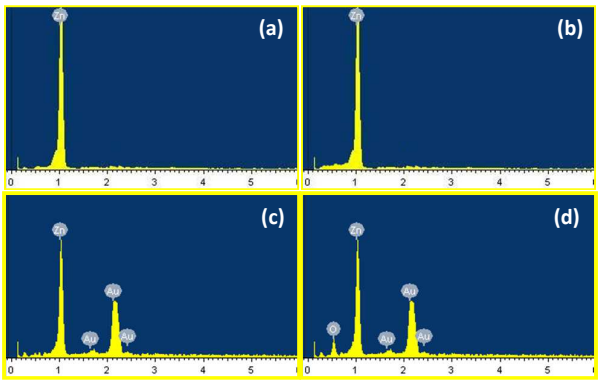

Fig. 4. EDS spectra: (a) sample 1, (b) sample 2, (c) sample 3 and (d) sample 4.

EDS analysis. In order to preliminarily confirm the surface elemental compositions, EDS spectra were performed firstly as shown in Fig. 4. The untreated zinc surface presented 99.97 atom% of zinc, indicating sample 1 was pure zinc substrate. After etching process, the surface composition of sample 2 was almost identical. Thus, etching process affected only the surface morphology, not the surface chemical environment. Before annealing treatment, surface compositions of sample 3 presented 75.97 atom% of zinc and 24.03 atom% of gold. After annealing treatment in an oven at 160℃ for 30 min, the compositions of sample 4 presented a slightly lower Zn content

of 45.91 atom% and Au content of 13.92 atom%. Besides, the appearance of 40.17 atom% of oxygen indicated the generation of oxide on the surface. This vibration of atom content implied that the compositions of sample surface 3 and 4 had significant changes before and after annealing treatment. Clearly, annealing treatment changed the surface chemical environment to be complicated, which favoured the surface characteristic to be superhydrophobic.

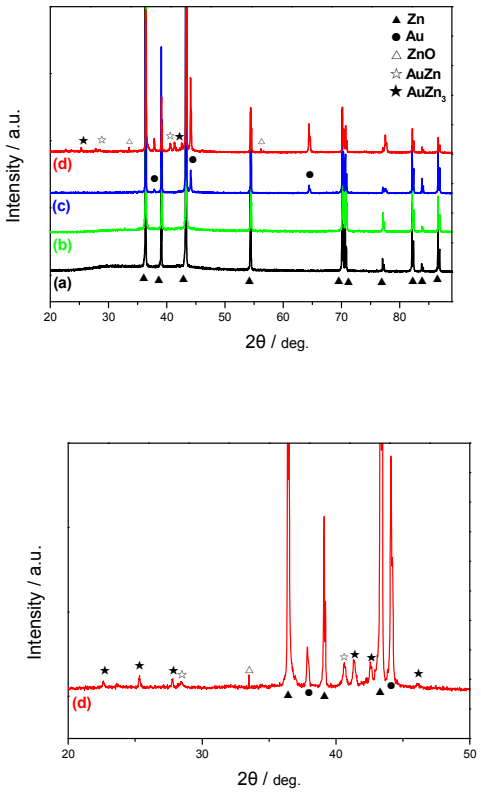

Fig. 5. XRD spectra: (a) untreated zinc surface (black line), (b) sample surface after etching process (green line), (c) sample surface after immersion process (blue line), (d) sample surface after annealing treatment (red line).

XRD analysis. XRD spectra were conducted to analyze the surface substance of sample 1, 2, 3, and 4 as shown in Fig. 5. The symbols of ▲ and ● represent the peaks of Zn and Au respectively. The sharp peaks of Zn(002), Zn(100), Zn(101), Zn(102), Zn(103), Zn(110), Zn(004), Zn(112), Zn(200) and Zn(201) were attributed to pure zinc on Zn substrate, which were in accord with the JCPDS card No. 65-3358 perfectly as shown in Fig. 5(a). After etching process as shown in Fig. 5(b), positions of peaks kept unchanged, and no new peaks were generated, indicating that the etching process only increased the surface roughness rather than changing the surface compositions. After immersion process as shown in Fig. 5(c), three new peaks appeared at 2θ = 37.85º, 44.10º and 64.46º respectively, which were respectively assigned to the characteristic peaks of Au(111), Au(200) and Au(220) planes of the metallic Au crystals (JCPDS card No. 65-2870). The intensity of Au(200) peak was evidently stronger than that of other peaks, indicating a preferential growth of Au crystals along the (200) plane. After annealing treatment as shown in Fig. 5(d), a large number of new peaks generated. The symbols of △, ☆ and ★ represent the peaks of ZnO, AuZn and $AuZn_3$ alloy respectively. The peaks at 2θ = 33.49º and 56.16º were assigned to the characteristic peaks of ZnO(111) and ZnO(220) respectively (JCPDS card No. 65-2880). To observe the new peaks clearly, sample 4 with range of 20º to 50º in the vertical axis was magnified. The peaks at 2θ = 28.43º and 40.62º were in accord with the characteristic peaks of AuZn(100) and AuZn(110) respectively (JCPDS card No. 65-0435). The other peaks at 2θ = 22.60º, 25.30º, 27.78º, 41.27º, 42.69º and 46.01º were assigned to the characteristic peaks of $AuZn_3$(200), $AuZn_3$(210), $AuZn_3$(211), $AuZn_3$(320), $AuZn_3$(321) and $AuZn_3$(400) planes of the alloy $AuZn_3$ crystals (JCPDS card No. 65-1849). These data accorded with the XRD results of Au-Zn alloys reported by Gotzmann[37] and Borissov[38] perfectly. The generation of oxide and intermetallic compounds via annealing treatment changed the surface chemical environment, resulting in the surface wettability transforming from superhydrophilicity to superhydrophobicity.

XPS analysis. In order to further elaborate the effect of annealing treatment and to obtain detailed information on the chemical states of ions, XPS spectra were performed as shown in Fig. 6. Binding energy was calibrated by taking the C 1s peak (285 eV) as a reference. Fig. 6(a) shows the general survey spectra of the surface before and after annealing treatment, which displays that both of the surfaces contain Zn, Au, O, and C. The photoelectron peak for C 1s indicates the existence of a small amount of carbon element, which may probably be attributed to contamination caused by specimen handling or by pumping oil used in the XPS instrument itself.[39] Typical high resolution scans of Zn 2p, Au 4f - Zn 3p and O 1s were shown in Fig. 6(b), (c) and (d), respectively.

In the Zn region as shown in Fig. 6(b), before annealing treatment (curve A), the binding energy of the Zn 2p 3/2 and Zn 2p 1/2 peaks were centered at 1021.6 eV and 1044.7 eV respectively, according with Wertheim's[40] results perfectly. After annealing treatment, those of the curve B decreased slightly to 1021.3 eV (Zn 2p 3/2) and 1044.4 eV (Zn 2p 3/2) respectively, and this tendency of lower binding energy was similar to the XPS study of Cu-Zn alloy system by Wertheim's[40] group.

The Au 4f - Zn 3p peaks as shown in Fig. 6(c) can be deconvoluted by means of a standard software using a Shirley type background correction and symmetric Gaussian curves. Before annealing treatment (curve A) as shown in Fig. (e), four separate peaks were resolved, namely Au 4f 7/2 (83.4 eV), Au 4f 5/2 (87.0 eV) for gold, and Zn 3p 3/2 (88.6 eV) and Zn3p 1/2 (91.6 eV) for zinc. This result was in accord with the XPS study of Au-ZnO nanowire films by Jamali-Sheini *et al.*[41] However, after annealing treatment (curve B) as shown in Fig. (f), only three separate peaks can be disassembled, namely Au 4f (84.3 eV) for gold, and Zn 3p 3/2 (88.4 eV) and Zn 3p 1/2 (91.4 eV) for zinc. The Au atoms have Zn as nearest neighbours, which will to some extent localize the Au like bands. On the low binding energy side, only one peak can be attributed to Au, and this may be due to the generation of Au-Zn alloys, which was similar to the XPS result of AuZn alloy by Leiro *et al.*[42] Valence band and core electron spectra obtained by X-ray photoelectron spectroscopy (XPS) have provided insight into charge transfer in alloy systems.[40]

The scan of the O 1s spectrum was shown in Fig. 6(d). Before annealing treatment (curve A), the asymmetric peak was deconvoluted into two components with binding energies of 530.3 eV and 531.8 eV, which can be attributed to the formation of O-Zn

and O-H bonds, respectively. The O-H bond can be attributed to formation of loosely bound oxygen on the surface (absorbed oxygen and O-H groups) or to O^{2-} ions in the oxygen-deficient regions.[43,41] After annealing treatment (curve B), deconvolution showed binding energies of two overlapping components were 530.2 eV and 531.3 eV respectively. In addition, we can clearly see that the intensity of shoulder peak at the higher binding energy reduced obviously after annealing treatment, indicating the fading of absorbed oxygen and O-H groups, or the decreasing of oxygen-deficient regions. Formation of O-Zn bond was attributed to O^{2-} ions in the ZnO lattice.

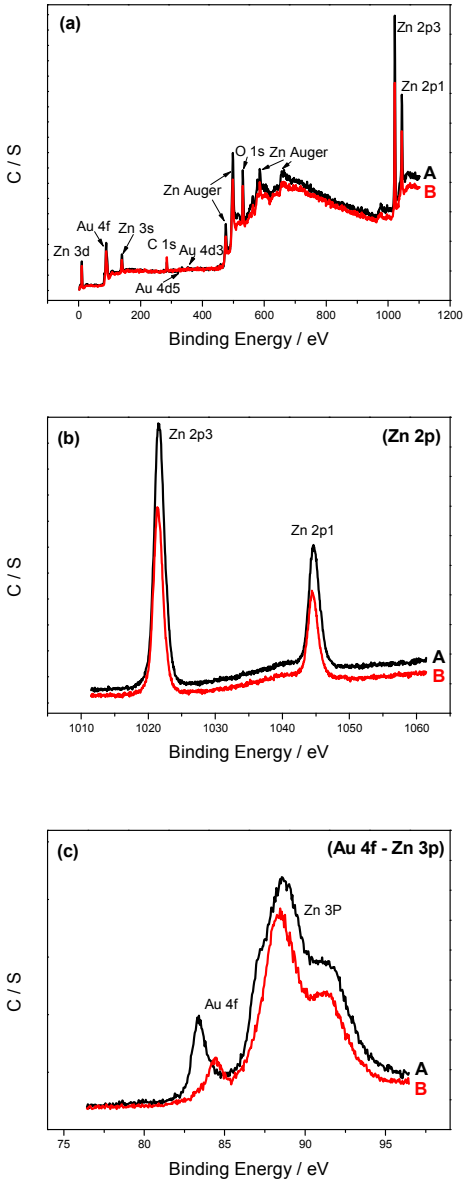

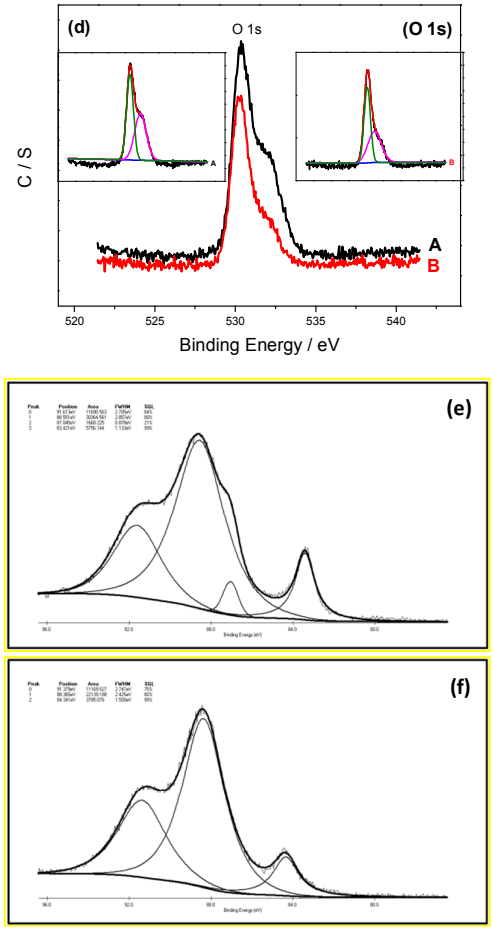

Fig. 6. XPS spectra: (a) the total region, (b) Zn 2p region, (c) Au 4f - Zn 3p region, (d) O 1s region, (e) fitted curve of (A) in (c), (f) fitted curve of (B) in (c); (A) before annealing treatment (black line), (B) after annealing treatment (red line). The insets of (d) are fitted curves of (A) and (B), respectively.

Effects of etch and immersion process on wettability

Based on the analysis above, the important effect of annealing treatment on wettability can be verified, which changed the surface chemical environment and surface morphologies. Then, we decided to discuss the effects of etch and immersion process respectively. So, the sample 5 (without immersion process) and sample 6 (without etch process) were prepared to be analyzed in comparison with sample 4 (the superhydrophobic surface).

Surface morphology and wettability. Fig. 7 shows the SEM images and its corresponding water CAs on the surfaces of sample 5 and 6 respectively. The static WCA of sample 5 was about 109 ±2°, indicating hydrophobicity, and there were lots of holes on the surface as shown in Fig. 7(a). The magnification as shown in Fig. 7(b) showed some layers of membranes covered on the surface and connected the holes, and this may be due to the generation of zinc oxide via annealing treatment. Surprisingly, there were many spherical structures on the surface of sample 6 but not the dendritic structures like sample 4 as shown in Fig. 7(c). The size of these spheres was about 2-5 μm and some of them got together, which can be clearly seen from the magnification as shown in Fig. 7(d). The water droplets stuck on the surface with a water CA of 122 ±2°.

Based on the wettability, the immersion process may be more important than the etch process. Of course, for superhydrophobicity, both of them are indispensable and crucial.

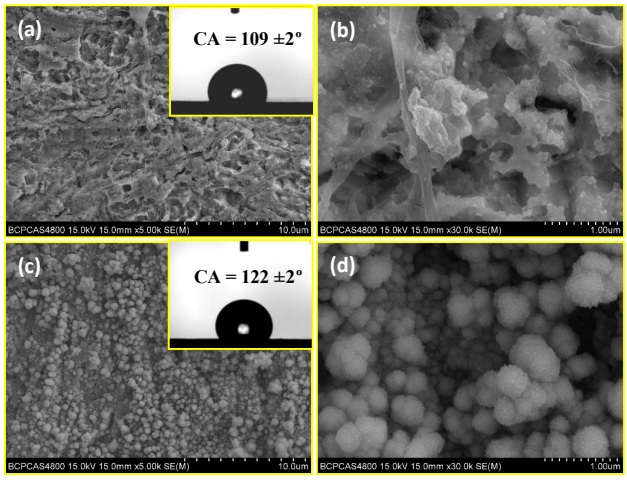

Fig. 7. SEM images of sample 5 (a and b) and 6 (c and d). The insets are the corresponding water CAs. The magnification of (a), (c) is × 5 K and that of (b), (d) is × 30 K.

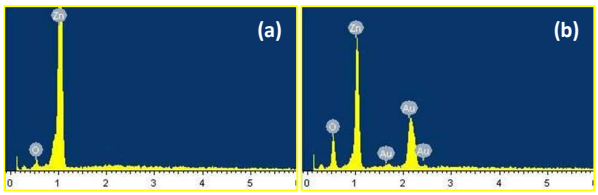

Fig. 8. EDS spectra of sample 5 (a) and sample 6 (b).

EDS analysis of sample 5 and 6. From the EDS spectra as shown in Fig. 8(a), we can clearly see that there were zinc and oxygen on the surface of sample 5, indicating the existence of zinc oxide. The surface of sample 6 presented 37.86 atom% of zinc, 8.79 atom% of gold and 53.35 atom% of oxygen as shown in Fig. 8(b). The atom content of gold on the surface of sample 6 was distinctly less than that of sample 4, indicating etch process was in favour of the deposition of gold, and also affected the surface morphologies of gold significantly. Both of the surface chemical environment and surface morphology impact the wettability, so we will further analyze the surface compositions.

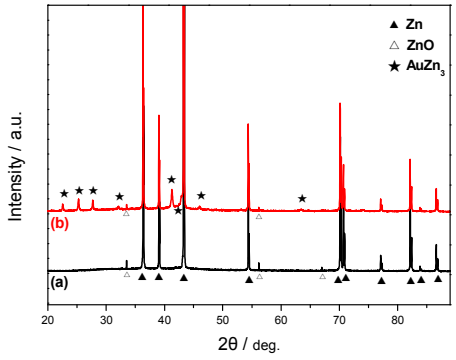

Fig. 9. XRD spectra of sample 5 (a) and sample 6 (b).

XRD analysis of sample 5 and 6. In order to further explain the surface composition of sample 5 and 6, XRD spectra were performed as shown in Fig. 9. The symbols of ▲, △ and ★ represent the peaks of Zn, ZnO and $AuZn_3$ alloy respectively. The sharp peaks of Zn were obvious and distinct, which were attributed to the pure zinc on Zn substrates (JCPDS card No. 65-3358). The peaks at 2θ = 33.51°, 56.15° and 67.01° were assigned to the characteristic peaks of ZnO(111), ZnO(220) and ZnO(311) respectively (JCPDS card No. 65-2880), indicating a large amount of ZnO appeared on the etched zinc surface as shown in Fig. 9(a). The peaks as show in Fig. 9(b) at 2θ = 22.51°, 25.20°, 27.64°, 32.02°, 41.19°, 42.77°, 46.01° and 63.41° were assigned to the diffraction peaks of $AuZn_3$(200), $AuZn_3$(210), $AuZn_3$(211), $AuZn_3$(220), $AuZn_3$(320), $AuZn_3$(321), $AuZn_3$(400) and $AuZn_3$(520) respectively, which were in good agreement with $AuZn_3$ alloy crystallographic data (JCPDS card No. 65-1849). Interestingly, the peaks of Au and AuZn alloy did not appear clearly or were not detected in the 2θ scan range of 20-90°. This meant most deposited gold transformed into intermetallic compound $AuZn_3$ alloy. As is known to all, the surface chemical environment is vital for superhydrophobicity. The most excellent superhydrophobicity belongs to sample 4, in which Au, AuZn alloy, $AuZn_3$ alloy and a few ZnO on the surface can be detected distinctly as shown in Fig. 5(d). Moreover, the surface morphology plays a more important role in fabricating superhydrophobic surface and obviously, the dendritic structures have more advantages than the spherical structures.

Theoretical mechanism for superhydrophobicity

Combining with the analyses of SEM, EDS, XRD and XPS above, the formation mechanism of the as-prepared superhydrophobic surface can be concluded and all the reactions involved are listed in Scheme 1. While the zinc substrates were immersed in 1 mol/L NaOH aqueous solution for 5 min, the surfaces were instantaneously damaged and etched by OH^- ions. Some holes and cracked surface textures appeared, which could be clearly seen from the SEM as shown in Fig. 2(b). Then when the surfaces were immersed in 5 mmol/L $HAuCl_4$ aqueous solution for 20 min, H^+ ions reacted with the zinc surfaces to generate the Zn^{2+} ions; at the same time, $AuCl_4^-$ ions came in contact with the zinc surfaces and consequently reacted with the Zn to form Zn^{2+} ions and elemental Au. A large number of Au deposited on the zinc surface, which could be clearly seen from Fig. 2(c). Owing to the standard electrode potentials of Zn/Zn^{2+} and $AuCl_4^-/Au$ were 0.7618 V and 1.002 V respectively, so the chemical substitution reaction can occur spontaneously in the air. Finally, when the substrates were annealed in an oven at 160℃ for 30 min, some exposed zinc was gradually oxidized to ZnO; some zinc and deposited gold were integrated into intermetallic compounds, namely AuZn and $AuZn_3$ alloys. The surface chemical environment was important for wettability. The generation of alloys and oxide via annealing treatment, which changed the surface chemical composition, was one of the critical factors for the surface characteristic transforming from superhydrophilicity to superhydrophobicity.

$$Zn + 2OH^- \rightarrow ZnO_2^{2-} + H_2\uparrow \quad (1)$$

$$Zn + 2H^+ \rightarrow Zn^{2+} + H_2\uparrow \quad (2)$$

$$3Zn + 2AuCl_4^- \rightarrow 3Zn^{2+} + 2Au + 8Cl^- \quad (3)$$

$$2Zn + O_2 \rightarrow 2ZnO \quad (4)$$

$$Zn + Au \rightarrow AuZn \quad (5)$$

$$3Zn + Au \rightarrow AuZn_3 \quad (6)$$

Scheme 1. The main reactions in the formation of superhydrophobic surface.

Theoretical explanation for wettability

For expounding the aforesaid characteristics of different sample surfaces (here only the special sample 3 with superhydrophilicity and sample 4 with superhydrophobicity will be discussed), two theories (the Wenzel[10] and the Cassie-Baxter[11]) are considered. These models explain the effect of roughness on the apparent contact angle of liquid drops.[44,45] The Wenzel model recognizes that surface roughness increases the available surface area of the solid, which modifies the surface contact angle according to the expression

$$\text{Cos } \theta^* = r \text{ Cos } \theta \quad (7)$$

where θ^* is the apparent contact angle on a rough surface, θ is the equilibrium contact angle on a smooth surface, and r is the surface roughness defined as specific area ratio between the real and projected solid-liquid contact area.

The surface characteristic of sample 3 is completely superhydrophilic and the water droplet is totally sticky to the surface, so the Wenzel state is applicable. Here, given that $\theta^* = 4^o$ and $\theta = 54^o$, and r is calculated as 1.697. That is, the value of real solid-liquid contact area is as 1.697 times as that of the projected on the superhydrophilic surface. This result accords with the assumption that hydrophilicity of hydrophilic surface and hydrophobicity of hydrophobic surface increases as roughness increases. Of course, the adhesion between the droplet and surface is also enhanced.

The Cassie-Baxter model, on the other hand, postulates that the superhydrophobic nature of a rough surface is caused by microscopic pockets of air remaining trapped below the liquid droplet, leading to a composite interface.[44] This state can be defined as follows:

$$\text{Cos } \theta^* = f_1 \text{ Cos } \theta - f_2 \quad (8)$$

Where θ^* and θ represent the apparent contact angle on a rough surface and the equilibrium contact angle on a smooth surface respectively; f_1 and f_2 are the area fractions of the solid and air on the surface respectively and $f_1 + f_2 = 1$. This theory demonstrates that a liquid droplet sits on asperities generating air cavities and giving rise to decrease in solid-liquid interface and increase in liquid-vapour interface.[46,47]

The water droplet on the surface of sample 4 is completely superhydrophobic and there is no sticky behaviour with a water sliding angle of approximately 0°, indicating that microscopic pockets of air may be trapped below the water droplet. Therefore, the Cassie-Baxter state is considered. Given that $\theta^* = 170^o$ and $\theta = 54^o$, f_1 and f_2 are estimated as 0.010 and 0.990 respectively. These data indicate that when a water droplet is placed on a superhydrophobic surface, approximately 1.0 % serves as the contact area of the water droplet and the solid surface, and the remaining 99.0 % serves as the contact area of the water droplet and air. Consequently, the liquid droplet is non-sticky to the surface and the adhesion between droplet and surface is low. This leads to the roll-down property of the water droplet on the superhydrophobic surface.

Roll-down property of the superhydrophobic surface

Because of the non-sticky behaviour of water droplet on the superhydrophobic surface in Cassie-Baxter state, the water droplet rolled down easily from the surface. We investigated that a water droplet of 8 μL on the as-prepared superhydrophobic surface could easily move and bounce as shown in Fig. 10 (see Video S1 in Supplementary Information) on horizontal surface. Moving on the surface, the water droplet did not adhere to the surface. We found also that the similar consequence emerged when a water droplet dispensed on the slightly titled surface. The roll-down property of the superhydrophobic surface may facilitate its potential and practical applications.

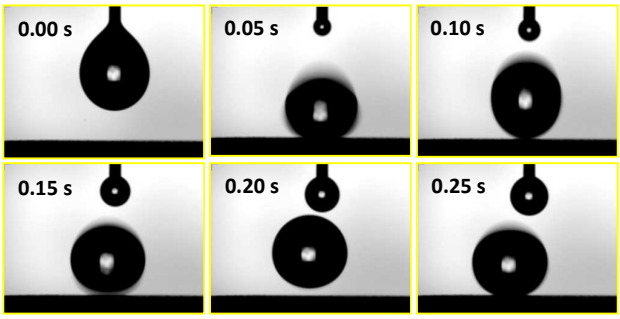

Fig. 10. Successive snapshots of an 8 μL droplet on the superhydrophobic surface.

Self-cleaning property of the superhydrophobic surface

Fig. 11. Self-cleaning property test: soils loaded superhydrophobic surface is cleaned by moving water droplets (a); soils loaded untreated zinc surface is rushed by moving water droplets (b).

Superhydrophobic surfaces with self-cleaning ability have become a leading research topic in surface science and technology due to their various potential and practical applications.[48-51] In the following experiment, we presented the self-cleaning property of the superhydrophobic surface. Water droplets were dispensed on the horizontal superhydrophobic surface heavily loaded with dust particles (in our case we used soil powder). As the water droplets rolled down guided by the tip of a micropipette, soil powder were removed adequately as shown in Fig. 11(a) (see Video S2 in Supplementary Information). As a result, the dirty surface became a cleaned surface. Moreover, the investigation was carried out by dispensing water droplets on the horizontal untreated zinc surface adhered soil powder as comparisons. As a result, the soil powder was not removed by the rolled-down water droplets as we would think as shown in Fig. 11(b) (see Video S3 in Supplementary Information). The water droplets and soil powder remained and adhered to the zinc surface. The self-cleaning character of

superhydrophobic surface could be applied to protect surface or material from dirty and might have important potential applications.

Anti-corrosion property of the superhydrophobic surface

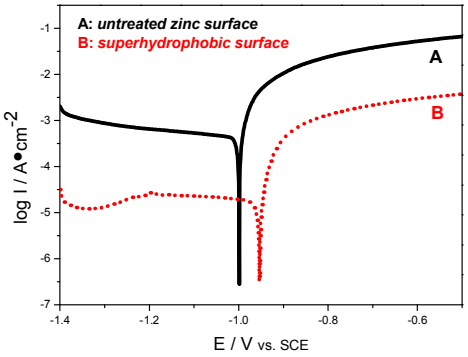

Fig. 12. Potentiodynamic polarization curves of the untreated zinc surfaces (A) and the resulting superhydrophobic surfaces (B) in 3.5 wt% NaCl aqueous solution.

To date, the polarization curve was a useful tool in determining the corrosion rate of a substrate. In a typical polarization curve, a lower corrosion current density or a higher corrosion potential corresponded to a lower corrosion rate and a better corrosion resistance.[52] Potentiodynamic polarization curves of the untreated zinc surface and the resulting superhydrophobic surface in 3.5 wt% NaCl aqueous solution were obtained using the Tafel extrapolation method and were presented in Fig. 12. A close inspection of the data revealed that the corrosion potential (E_{corr}) and corrosion current density (I_{corr}) of the untreated zinc surface were -1.000 V and 1.865 $\times$ 10^{-3} A/cm^2 respectively. Obviously, the corrosion potential of the resulting superhydrophobic surface was more positive than that of the untreated zinc surface, with a value of -0.954 V. The shift of E_{corr} to more positive direction might be linked to an improvement in the protective property of the superhydrophobicity formed on zinc substance.[6] It should be noted that the corrosion current density of the resulting superhydrophobic surface was about 1.822 $\times$ 10^{-5} A/cm^2, which was reduced by more than 2 order of magnitude comparing with that of the untreated zinc surface and this should owe to the contribution of Au-Zn alloys on the surface. Such low current density indicated an excellent corrosion resistance for the superhydrophobic surface.

Tribological study of the superhydrophobic surface

A dynamic load ranged from 5 N to 20 N was used in the scratch test to analyze the bonding strength between the superhydrophobic coating and the substrate. For composite surface, the critical load appeared at the point, where the coefficient of friction (COF) values abruptly changed. This critical load indicated the transition of the wear regime from one material to another, and that the superhydrophobic coating was completely peeled off from the substrate surface. The variation in COF with load for superhydrophobic surface was shown in Fig. 13. It was noticeable that there was an abrupt change of the COF at load about 10 N. Another change in COF curve clearly occurred before seizure of 20 N. We can clearly see that the critical load was about 10 N, and this value was better than 6 N in our previous reports.[15] This superhydrophobic surface exhibited good binding ability, and this should be attributed to the annealing treatment, which led to the generation of Au-Zn alloys, and then enhanced the binding force and affinity between substrate and coating. This excellent mechanical property of the superhydrophobic surface was important for its various applications, such as self-cleaning and anti-corrosion properties, and might provide more values for its potential applications.

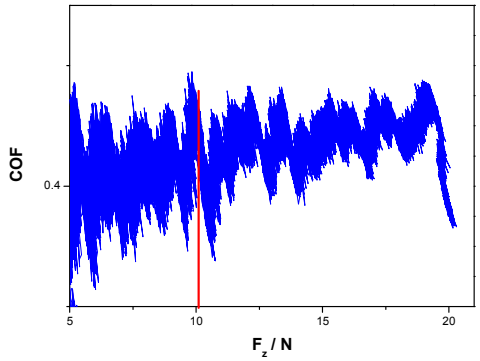

Fig. 13. The variation in coefficient of friction (COF) with load for superhydrophobic surface.

Conclusions

In summary, firm superhydrophobic Au-Zn alloys surfaces have been fabricated successfully on zinc substrate via chemical substitution deposition and subsequent annealing treatment. The resulting surfaces exhibited remarkable superhydrophobicity with WCA of 170 ±2° and WSA smaller than 1° without any organic modification. Both of the generation of Au-Zn alloys (including $AuZn_3$ and AuZn) and ZnO, and the surface micro-/nano- binary architectures were important for superhydrophobicity. The resulting suprehydrophobic Au-Zn alloys surfaces exhibited exquisite roll-down, self-cleaning, and excellent anti-corrosion abilities, and also had firm mechanical property about 10 N. The corrosion current density of the resulting superhydrophobic surface was reduced by more than 2 order of magnitude comparing with that of the untreated zinc surface and this should owe to the contribution of Au-Zn alloys on the surface. The convenient preparation process and excellent properties of the resulting suprehydrophobic Au-Zn alloys surfaces can offer an effective strategy for fabricating superhydrophobic surfaces on various metallic materials and also have important values for more potential applications.

Acknowledgements

We gratefully acknowledge the National Natural Science Foundation of China (No. 21271027) for this work.

References

1 H. Zhu, Z.G. Guo and W.M. Liu, *Chem. Commun.*, 2014, **50**, 3900.
2 H. Bellanger, T. Darmanin, E.T. Givenchy and F. Guittard, *Chem. Rev.*, 2014, **114**, 2694.
3 K.S. Liu, M.Y. Cao, A. Fujishima and L. Jiang, *Chem. Rev.*, 2014, **114**, 10044.

4 R.J. Liao, Z.P. Zuo, C. Guo, A.Y. Zhuang, Y. Yuan, X.T. Zhao and Y.Y. Zhang, *Cold Reg. Sci. Technol.*, 2015, **112**, 87.
5 N. Wang, D.S. Xiong, Y.L. Deng, Y. Shi and K. Wang, *ACS Appl. Mater. Interfaces*, 2015, **7**, 6260.
6 Y.Y. Cheng, S.X. Lu, W.G. Xu and H.D. Wen, *RSC Adv.*, 2015, **5**, 15387.
7 P.V. Mahalakshmi, S.C. Vanithakumari, J. Gopal, U. Kamachi Mudali and Baldev Raj, *Current Science*, 2011, **101**, 1328.
8 X. Li, M. Wang, C. Wang, C. Cheng and X.F. Wang, *ACS Appl. Mater. Interfaces*, 2014, **6**, 15272.
9 M.B. Oliveira, A.L. Neto, C.R. Correia, M.L. Rial-Hermida, C. Alvarez-Lorenzo and J.F. Mano, *ACS Appl. Mater. Interfaces*, 2014, **6**, 9488.
10 R.N. Wenzel, *Ind. Eng. Chem.*, 1936, **28**, 988.
11 A.B.D. Cassie and S. Baxter, *Trans. Faraday Soc.*, 1944, **40**, 546.
12 N. Zhang, S.X. Lu, W.G. Xu and Y. Zhang, *New J. Chem.,* 2014, **38**, 4534.
13 H.Y. Gao, S.X. Lu, W.G. Xu, S. Szunerits and R. Boukherroub, *RSC Adv.*, 2015, **5**, 40657.
14 U.P. Shaik, D.D. Purkayastha, M.G. Krishna and V. Madhurima, *Appl. Surf. Sci.*, 2015, **330**, 292.
15 G. He, S.X. Lu, W.G. Xu, S. Szunerits, R. Boukherroub and H.F. Zhang, *Phys. Chem. Chem. Phys.,* 2015, **17**, 10871.
16 D.A. Wang, Y. Liu, X.J. Liu, F. Zhou, W.M. Liu and Q.J. Xue, *Chem. Commun.*, 2009, 7018.
17 X. Gao, X. Yao and L. Jiang, *Langmuir*, 2007, **23**, 4886.
18 N. Chadwick, S. Sathasivam, A. Kafizas, M.S. Bawaked, Y.A. Obaid, S. Al-Thabaiti, N.S. Basahel, P.I. Parkin, and J.C. Carmalt, *J. Mater. Chem. A*, 2014, **2**, 5108.
19 J. Zhao, B.X. Leng, Z.Z. Shao, Gijsbertus de With and W.H. Ming, *RSC Adv.*, 2013, **3**, 22332.
20 X.F. Shi, S.X. Lu and W.G. Xu, *Materials Chemistry and Physics*, 2012, **134**, 657.
21 P. Guo, S.R. Zhai, Z.Y. Xiao and Q.D. An, *Journal of Colloid and Interface Science*, 2015, **446**, 155.
22 T.C. Wang, L.J. Chang B. Hatton, J. Kong, G. Chen, Y. Jia, D.S. Xiong and C.P. Wong, *Materials Science and Engineering: C*, 2014, **43**, 310.
23 Y. Wang, X.W. Liu, H.F. Zhang and Z.P. Zhou, *RSC Adv.*, 2015, **5**, 18909.
24 R. Abbas, M.A. Khereby, W.A. Sadik and A.G.M. El Demerdash, *Cellulose*, 2015, **22**, 887.
25 J. Li, Z.J. Jing, Y.X. Yang, Q.T. Wang and Z.Q. Lei, *Surface and Coatings Technology*, 2014, **258**, 973.
26 J. Sun, F.D. Zhang, J.L. Song, L. Wang, Q.S. Qu, Y. Lu and L. Parkin, *Appl. Surf. Sci.*, 2014, **315**, 346.
27 H. Li, S.R. Yu, X.X. Han, E.Y. Liu and Y. Zhao, *Colloids and Surfaces A: Physicochemical and Engineering Aspects*, 2015, **469**, 271.
28 H.J. Wang, Z. Yang, J. Yu, Y.Z. Wu, W.J. Shao, T.T. Jiang and X.L. Xu, *RSC Adv.*, 2014, **4**, 33730.
29 Y.D. Zhang and L.W. Mi, *Chemistry Letters*, 2012, **41**, 915.
30 Z.G. Guo, W.M. Liu and B.L. Su, *Journal of Colloid and Interface Science*, 2011, **353**, 335.
31 B. Bhushan, Y.C. Jung and K. Koch, *Phil. Trans. R. Soc. A*, 2009, **367**, 1631.
32 J.L. Yong, Q. Yang, F. Chen, D.S. Zhang, G.Q. Du, J.H. Si, F. Yun and X. Hou, *J. Micromech. Microeng.*, 2014, **24**, 035006.
33 L. Feng, S.H. Li, Y.S. Li, H.J. Li, L.J. Zhang, J. Zhai, Y.L. Song, B.Q. Liu, L. Jiang and D.B. Zhu, *Adv. Mater.*, 2002, **14**, 1857.
34 D. Zhong, Q.L. Yang, L. Guo, S.X. Dou, K.S. Liu and L. Jiang, *Nanoscale*, 2013, **5**, 5758.
35 N.D. Boscher, V. Vaché, P. Carminati, P. Grysan and P. Choquet, *J. Mater. Chem. A*, 2014, **2**, 5744.
36 T.Y. Lo, Y.C. Huang, Y.N. Hsiao, C.G. Chao, W.T. Whang, *Surface & Coatings Technology*, 2014, **258**, 310.
37 K. Gotzmann, U. Burkhardt, M. Ellner and Y. Grin, *Powder Diffraction*, 1997, **12**, 248.
38 D. Borissov, A. Pareek, F.U. Renner and M. Rohwerder, *Phys. Chem. Chem. Phys.*, 2010, **12**, 2059.
39 K.W, Yao, S. Jaenicke, J.Y. Lin and K.L. Tan, *App. Catal. B: Environ.*, 1998, **16**, 291.
40 G.K. Wertheim, M. Campagna and S. Hiifner, *Phys. Eond. Matter.*, 1974, **18**, 133.
41 F. Jamali-Sheini, R. Yousefi, K.R. Patil, *Ceramics International*, 2012, **38**, 6665.
42 J.A. Leiro, K. Kokko and R. Laihia, *Journal of Electron Spectroscopy and Related Phenomena*, 2001, **113**, 167.
43 A.B. Djurisic, Y.H. Leung, K.H. Tam, Y.F. Hsu, L. Ding, W.K. Ge, Y.C. Zhong, K.S. Wong, W.K. Chan, H.L. Tam, K.W. Cheah, W.M. Kwok and D.L. Phillips, *Nanotechnology*, 2007, **18**, 095702.
44 A. Tuteja, W. Choi, M.L. Ma, J.M. Mabry, S.A. Mazzella, G.C. Rutledge, G.H. McKinley and R.E. Cohen, *Science*, 2007, **318**, 1618.
45 L. Gao and T.J. McCarthy, *Langmuir*, 2007, **23**, 3762.
46 H. Bellanger, T. Darmanin, T.E. de Givenchy and F. Guittard, *Chem. Rev.*, 2014, **114**, 2694.
47 Anup Kumar Sasmal, Chanchal Mondal, Arun Kumar Sinha, Samiran Sona Gauri, Jaya Pal, Teresa Aditya, Mainak Ganguly, Satyahari Dey and Tarasankar Pal, *ACS Appl. Mater. Interfaces*, 2014, **6**, 22034.
48 Q.F. Xu, J.N. Wang, K.D. Sanderson, *ACS Nano*, 2010, **4**, 2201.
49 C. Wang, T. Yao, J. Wu, C. Ma, Z. Fan, Z. Wang, Y. Cheng, Q. Lin and B. Yang, *ACS Appl. Mater. Interfaces*, 2009, **1**, 2613.
50 X. Li, C. Zhou, R. Du, N. Li, X. Han, Y. Zhang, S. An and C. Xiao, *ACS Appl. Mater. Interfaces*, 2013, **5**, 5430.
51 F. Su and K. Yao, *ACS Appl. Mater. Interfaces*, 2014, **6**, 8762.
52 J. Wang, D.D. Li, Q. Liu, X. Yin, Y. Zhang, X.Y. Jing and M.L. Zhang, *Electrochim. Acta*, 2010, **55**, 6897.

Superhydrophobic Au-Zn alloys surfaces with stable Cassie-Baxter state have been fabricated via immersion and anneal without any organic modification.